Microbial Pathogenesis 210 (2026) 108182

Contents lists available at ScienceDirect

Microbial Pathogenesis

journal homepage: www.elsevier.com/locate/micpath

Bioactive constituents from *Gardenia aqualla* (Rubiaceae) stem bark as promising antibacterial agents: *In vitro* and *in silico* insights

Jean Noël Nyemb [a,*], Gaetan Bayiha Ba Njock [b], Taye B. Demissie [c], Japheth O. Ombito [c], Syeda Abida Ejaz [d], Hafiz Muhammad Attaullah [d], Céline Henoumont [e], Sophie Laurent [e], Alembert Tiabou Tchinda [f], Emmanuel Talla [g,h], Marcello Iriti [i,**]

[a] Department of Refining and Petrochemistry, National Advanced School of Mines and Petroleum Industries, The University of Maroua, P.O. Box 08, Kaélé, Cameroon
[b] Department of Chemistry, Faculty of Science, The University of Maroua, P.O. Box 814, Maroua, Cameroon
[c] Department of Chemistry, Faculty of Science, University of Botswana, P/Bag 00704, Gaborone, Botswana
[d] Department of Pharmaceutical Chemistry, Faculty of Pharmacy, The Islamia University of Bahawalpur, Bahawalpur, 63100, Pakistan
[e] Department of General, Organic and Biomedical Chemistry, Faculty of Medicine and Pharmacy, University of Mons, NMR and Molecular Imaging Laboratory, B-7000, Mons, Belgium
[f] Institute of Medical Research and Medicinal Plants Studies (IMPM), Ministry of Scientific Research and Innovation, P.O. Box 6163, Yaounde, Cameroon
[g] Department of Chemistry, Faculty of Science, The University of Ngaoundere, Ngaoundere, Cameroon
[h] Department of Chemical Engineering, School of Chemical Engineering and Mineral Industries, The University of Ngaoundere, Ngaoundere, Cameroon
[i] Department of Biomedical, Surgical and Dental Sciences, University of Milan, 20129, Milan, Italy

ARTICLE INFO

Keywords:
Rubiaceae
Gardenia aqualla
Apocarotenoids
Antibacterial activity
Molecular docking

ABSTRACT

Continuing phytochemical investigation of the methanolic extract of *Gardenia aqualla* stem bark led to the isolation of a new fatty acid ester, henpentacontyl acetate (**1**), together with four known compounds: *trans*-apo-8′-carotenoic acid (**2**), ethyl (all-*E*)-8′-*trans*-apo-*β*-caroten-8′-oate (**3**), D-mannitol (**4**), and 2,3,4,5,6-pentahydroxyhexyl acetate (**5**). Acetalation of D-mannitol afforded a new derivative, 1,2:5,6-di-*O*-isopropylidene-D-mannitol (**4a**). The structures of all isolated and synthesized compounds were established by spectroscopic and spectrometric analyses and comparison with literature data. The antibacterial potential of compounds **1**–**5** was assessed *in vitro* using the microdilution method against Gram-positive and Gram-negative bacteria. Compounds **2** and **3** exhibited significant activity against *Staphylococcus aureus* ATCC700698 and *S. aureus* NR46003 (MIC = 8 μg/mL), while other compounds showed low to moderate effects depending on the strain. Molecular docking analysis against *S. aureus* pyruvate kinase demonstrated that compounds **2** and **3** had higher binding affinities (−11.94 kcal/mol) than ciprofloxacin (−8.54 kcal/mol) and penicillin (−8.16 kcal/mol). ADMET predictions revealed that compound **1** possesses favorable pharmacokinetic and low-toxicity properties, whereas compounds **2** and **3** showed good drug-likeness but limited solubility. Compound **4a** exhibited improved pharmacokinetic parameters and an extended half-life, suggesting potential for further development. Collectively, these findings highlight the therapeutic promise of *G. aqualla* constituents, particularly compounds **2**, **3**, and **4a**, as antibacterial agents for managing oral and ear infections.

1. Introduction

Antimicrobial resistance (AMR) which occurs when changes in bacteria, fungi, parasites and viruses no longer respond to antimicrobial agents, has emerged as one of the leading public-health threats of the 21st century [1]. The global burden is considerable: in 2019 bacterial AMR was directly responsible for 1.27 million deaths, contributing to an estimated 4.95 million deaths overall, with projections of up to 10 million deaths per year by 2050 [1–3]. Given the substantial morbidity and mortality and the sluggish pipeline of novel antimicrobials, there is an urgent need to develop new, efficacious and affordable antimicrobial agents with broad biological spectrum (see Figs. 3–10).

* Corresponding author. Department of Refining and Petrochemistry, National Advanced School of Mines and Petroleum Industries, The University of Maroua, P.O. Box 08, Kaele, Cameroon.
** Corresponding author.
E-mail addresses: nyembjeannoel@gmail.com (J.N. Nyemb), marcello.iriti@unimi.it (M. Iriti).

https://doi.org/10.1016/j.micpath.2025.108182
Received 19 September 2025; Received in revised form 9 November 2025; Accepted 11 November 2025
Available online 12 November 2025

In response to this challenge, medicinal plants remain a promising source of novel antimicrobial scaffolds. The traditional pharmacopoeia offers a rich repository of biologically active compounds, and medicinal plants have long been explored for drug-development initiatives [4–8]. Among these plants, members of the family Rubiaceae stand out for their ethnopharmacological use in treating infectious ailments and other diseases [9,10]. The Rubiaceae family comprises trees, shrubs and grasses, roughly 637 genera and 13,000 species, primarily distributed in tropical regions [11–13]. Within this family, the genus *Gardenia* Ellis is one of the largest, with approximately 129 taxonomically accepted species indigenous to tropical and subtropical zones [14,15]. Prior investigations of extracts and secondary metabolites from *Gardenia* spp. have revealed a range of pharmacological activities including anticancer, antibacterial, antioxidant, antidiabetic, anti-HIV and anti-inflammatory effects [9,10,16,17].

Turning attention to our specific taxon, *Gardenia aqualla* (community name 'Dingale' in the Adamawa Region of Cameroon, in *Fulfulde*) is used by traditional healers for leprosy, oral and ear infections, dysmenorrhea, jaundice, ulcers, diabetes, and syphilis [18,19]. Our previous phytochemical studies on this species revealed the presence of acetogenins, sugars, triterpenoids and steroids, with interesting antimicrobial and α-glucosidase inhibitory activities [10,17]. More recently, the hydro-ethanolic and aqueous extracts of fresh leaves of *G. aqualla* were shown to contain significant polyphenolic and flavonoid contents and displayed antibacterial activity [20]. In parallel, studies on other *Gardenia* species (for example *G. jasminoides* essential oil) have demonstrated antimicrobial activities, including *in silico* docking investigations [21]. In the broader context, research on the Rubiaceae family continues to yield promising antimicrobial leads: for instance, a 2024 study on several Rubiaceae species confirmed significant inhibitory effects of ethanol extracts on *E. coli* and *B. subtilis* [22]. This underscores the rationale of leveraging Rubiaceae phytochemistry in drug-discovery pipelines.

Given the persistent escalation of AMR globally, and the ethnobotanical, phytochemical and preliminary antimicrobial evidence supporting *G. aqualla*, the present work aimed to isolate and identify additional antimicrobial compounds from the stem bark of *G. aqualla*. Specifically, this study involves the isolation and characterisation of compounds from this plant, evaluation of their *in vitro* antibacterial potential, followed by molecular docking screening and *in silico* ADMET (absorption, distribution, metabolism, excretion and toxicity) and drug-likeness prediction.

In recent years, the integration of *in vitro* and *in silico* approaches has become increasingly important in the discovery of antimicrobial leads from plant-derived or natural product scaffolds. For example [23], demonstrated how flavonoids can be analyzed using DFT, molecular docking, molecular dynamics simulation and ADMET profiling to explore potential inhibition of KRAS in human disease. Similarly, methodological advances in screening such as those described by Ref. [24] enable high-throughput microdilution and docking workflows for botanically-derived antibacterial agents. By incorporating these evolving methodologies into our work on *Gardenia aqualla*, we align with current best-practice in antimicrobial drug-discovery and strengthen the scientific basis for our extraction, isolation, antibacterial screening and *in silico* modelling strategy.

2. Materials and methods

2.1. General experimental procedures

The NMR experiments were recorded using both a Varian Mercury Plus and a Bruker Avance AV-500 spectrometers (500 MHz for ^{1}H and 125 MHz for ^{13}C) with deuterated solvents ($CDCl_3$ and DMSO-d_6) using TMS as the internal reference. All chemical shifts are expressed in δ (ppm) and reported as s (singlet), d (doublet), dd (doublet of doublet), t (triplet), br (broad), and m (multiplet), respectively, and the coupling constants (*J*) are in Hz. Electrospray Ionization-Mass Spectrometry (ESI-MS) spectra were obtained from a Q-TOF Ultima spectrometer (Waters). Column chromatography was performed using silica gel 60 ASTM (70–230 and 230–400 Mesh). Precoated silica gel 60 F_{254} (Merck) plates were used to perform TLC. Mixture of *n*-hexane-EtOAc and EtOAc-MeOH were used as solvent for plates development. The spots were visualized under UV light, then by spraying with 50 % H_2SO_4 followed by heating for 10 min at 110 °C.

2.2. Plant material

The stem bark of *Gardenia aqualla* Stapf & Hutch were collected in the locality of Borongo in the Ngaoundere 3rd Subdivision, Region of Adamawa-Cameroon, in February 2022. After identification by identified by Mr Nana Victor, a botanist at the Cameroon National Herbarium (CNH), a voucher specimen where deposited at the CNH of Yaounde under the number 36894/HNC.

2.3. Extraction and isolation

Extracts where obtained from the powder (500 mg) of air-dried stem bark through a 72 h maceration in MeOH (2 L). The operation was repeated three times. After filtration with Whatman N°1 filter paper, the filtrates were collected, freed from solvent at 40°C under reduced pressure to give 49.85 g of crude MeOH extract. Approximately 40 g of this stem bark methanolic crude extract was subjected to a column chromatography (CC) on silica gel (70–230 mesh, ASTM) and eluted with *n*-hexane, mixtures of *n*-hexane/EtOAc, EtOAc and EtOAc/MeOH. Fractions of 250 mL were collected at the bottom of the column then pooled together into five major fractions (F_1-F_5) according to their TLC profile. Fraction F_4 (214.5 mg) was loaded onto a silica gel (230–400 mesh) CC and eluted with a gradient of EtOAc-MeOH (1:0–0:1) to yield compound **1** (6.7 mg). Fraction F_2 (528.3 mg) was subjected to another CC on silica gel (230–400 mesh) eluted with a gradient mode n-hexane-EtOAc (1:0 → 0:1) leading to four sub-fractions (F_{2A}-F_{2D}). Sub-fraction F_{2B} (85.4 mg) was further purified by a repeated CC of Sephadex LH-20 led to the isolation of compound **2** (8.1 mg) and compound **3** (10.5 mg). Fraction F_5 (3.08 g) was also further purified by silica gel (230–400 mesh) CC using a gradient elution (EtOAc-MeOH (1:0–0:1)) affording compound **4** (1.25 g) and **5** (15 mg).

2.4. Acetalation of compound *4*

Acetalation reaction is widely used to protect diols because acetals are known to be stable under various conditions and can easily be removed by hydrolysis in the presence of acid. In this study, we adopted the acetalation method developed by de Alvarenga et al. [25] with slight modifications. The method involves an excess of zinc chloride ($ZnCl_2$) in anhydrous acetone at room temperature and only hydroxyls at positions 1, 2, 5, and 6 are protected, leading to the formation of 1,2,5,6-di-*O*-isopropylidene-D-mannitol.

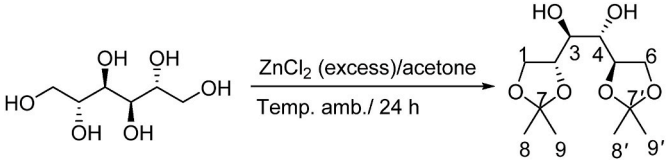

Briefly, 1 g of D-mannitol (5.5 mmol), 2 g of anhydrous $ZnCl_2$ (14.65 mmol) and 20 mL of anhydrous acetone were mixed in a 100 mL round bottom flask and stirred at room temperature until obtaining of a clear solution (24 h). The obtained clear solution was then poured into a Na_2CO_3 suspension (20 g in 20 mL H_2O) and stirred vigorously, then filtered, and the zinc carbonate washed with acetone (50 mL x 2) and filtered again. The filtrate was evaporated under reduce pressure to

remove acetone and residual water. The white solid obtained was dissolved in diethyl ether (60 mL) and transferred to a separating funnel. The organic phase was collected and the aqueous phase extracted with diethyl ether (3 x 60 mL). Solvent was removed under reduced pressure at room temperature to yield a white slurry. 100 mL of *n*-hexane was further added to this slurry and stirred for 20–30 min and then, the mixture was stored at −20 °C for 30 min and at 8 °C for another 30 min. After this time, the mixture was filtered under vacuum and the resulting solid washed with 100 mL of cold *n*-hexane. After 2–3 h of drying in a vacuum desiccator, diacetal **4a** (55 mg) was obtained.

2.5. Antimicrobial assay

2.5.1. Bacterial strains

Seven bacterial strains including Gram negative (*Escherichia coli* ATCC25922, *Shigella Sonnei* NR519, *Pseudomonas aeruginosa* ATCC9721, *Salmonella. Typhi* ATCC6539, *Klebsiella pneumonia* NR41916) and Gram positive (*Staphylococcus aureus* ATCC700698, *Staphylococcus aureus* NR46003) bacteria were used in the present study. These are clinical isolates provided by the "Centre Pasteur", Yaounde, Cameroon. All clinical strains were identified by biochemical and serological techniques [26].

2.5.2. Bioassay procedure

The antibacterial activity of the different compounds was evaluated by the microdilution method using the MTT (3-[4,5-dimethylthiazol-2-yl]-2,5-diphenyl tetrazolium bromide) colorimetric assay as described by Nyemb et al. [27] with slight modifications. Ciprofloxacin was used as standard drug for antibacterial assay. Samples were solubilized in DMSO 10 % before subjecting to a serial dilution ranged from 0.125 to 256 μg/mL in MHB. Precisely, compounds were firstly dissolved in 50 μL of DMSO 10 %, then 950 μL of MHB was added and solution obtained was serially diluted two fold in a 96-well microplate. 100 μL of bacterial suspensions in MHB was further introduced into each well to a final cell density of 1.5×10^6 CFU mL^{-1}. After incubation for 24 h at 37 °C, 40 μL of MTT solution (0.2 mg mL^{-1}) was added to each well and incubated for another 30 min. The MIC corresponding to the lowest concentration of extract or isolated compounds that does not produce any discoloration of the yellowish solution of MTT, was then registered. All the experiments were carried out in triplicate.

2.6. In silico studies

2.6.1. Molecular docking

To gain deeper insights into the biological activities, molecular docking simulations were conducted using AutoDock 4.2.6 Vina software [28] against *S. aureus* (PDB: 2w9h) and *P. aeruginosa LasR* (PDB: 2UV0). We selected these two antibacterial targets for the molecular docking studies due to their well-characterized structures and high docking suitability. Both have high-quality co-crystal that defines the pocket pharmacophore, enabling reliable receptor preparation and pose validation [29,30]. The grid center coordinates for both were set to 80, 80, and 80 in the x, y, and z axes, with a grid point spacing of 0.375 Å. The center of the grid box for *P. aeruginosa* was positioned at 24.771, 11.630, and 77.711 Å, where the active amino acids Leu36, Tyr47, Ile52, Tyr56, Trp60, Arg61, Tyr64, Asp73, Thr75, Ser129, Trp88, and Phe101 are located. In the case of *S. aureus*, the grid center was positioned at 9.393, −0.025, and 13.018 Å, where the active amino acids Leu5, Val6, Ala7, Leu20, Pro25, Asp27, Leu28, Val31, Ser49, Ile50, Arg57, Phe92, Thr111 are located. A total of 100 different conformations were generated for each targeted isolated compound to account for conformational flexibility during the docking process. The same other protocols to our previous works were followed [31–33]. The MGL 1.5.6 program was used to prepare the receptor molecules by removing the co-crystallized substrate and water Molecules. Polar hydrogens and Kollman charges were added during the protein cleaning process. Non-polar hydrogens were merged, and Gasteiger partial atomic charges were assigned. The structures of the isolated molecules were optimized using the B3LYP [34,35] functional and the 6-31+G (d,p) [36] basis set using the Gaussian 16 [37] program package. For all the atoms, standard docking parameters were used. To maximize the accuracy of the docking results, hundred alternative conformations for each of the molecules were produced by the Lamarckian genetic algorithm (LGA) software [38] with an adaptive whole method search in AutoDock [39]. The interactions between the active amino acids and the compounds were thoroughly analyzed to gain deeper insights into the molecular docking results. These interactions were visualized using the Discovery Studio program, which enabled a detailed examination of the binding modes. The analysis specifically focused on the conformers with the lowest binding free energy, as these represent the most stable and energetically favorable configurations. Through this visualization, key interactions such as hydrogen bonds, hydrophobic interactions, and electrostatic forces between the compounds and the active site residues were identified, providing a comprehensive understanding of the molecular recognition and binding affinity.

2.6.2. ADMET analysis

The physicochemical and pharmacokinetic properties of the isolated and the semisynthetic identified compounds were predicted using the online ADMETLAB 3.0 web server (https://admetlab3.scbdd.com/server/evaluationCal) [40]. By using an array of predictive models and sophisticated algorithms, to give a prognostic on both drug-likeness and potential toxicity [41], ADMETLAB facilitates a comprehensive evaluation of several pharmacokinetic parameters especially absorption, distribution, metabolism, excretion and toxicity (ADMET) [42].

3. Results and discussion

3.1. Phytochemical study

The MeOH extract of *G. aqualla* stem bark was subjected to repeated column chromatography over silica gel to afford a new ester, compound **1** along with four known compounds *trans-apo*-8′-carotenoic acid (**2**), ethyl (all *E*)-8′-*trans*-apo-*β*-caroten-8′-oate (**3**) [43]; [44]; [45], D-mannitol (**4**) [10] and 2,3,4,5,6-pentahydroxyhexyl acetate (**5**) [10]. In addition, an unprecedented mannitol derivative (**4a**) was obtained from acetalation of D-mannitol. The structures of all the compounds (Fig. 1) were determined based on a comparison of their spectroscopic and spectrometric data with those published in the literature (see Fig. 2).

Compound **1** was isolated as a white powder. It was assigned the molecular formula $C_{53}H_{106}O_2$ based on its (+ve) ESI-MS-TOF spectrum which showed a *pseudo*-molecular ion peak at *m/z* 792.6 $[M + NH_4]^+$ (calcd. *m/z* 792.9 for $C_{53}H_{106}O_2NH_4^+$), indicating one double bound equivalent. The ^{1}H NMR spectrum of compound **1** showed a triplet of two protons at δ_H 4.14 characteristic of an oxygen bearing methylene group. The ^{1}H NMR spectrum also displayed a signal of a singlet of three protons at δ_H 1.9 (3H, s) attributed to the methyl protons adjacent to a carbonyl group suggesting the presence of an ester group [10]. A broad signal ranging from δ_H 1.23 to 1.61 suggests the presence of a long hydrocarbon chain $(-CH_2-)_n$ and, a characteristic signal of a an angular methyl group was also noticed at δ_H 0.85 (3H, t). The ^{13}C NMR spectrum coupled to DEPT 135 spectrum showed characteristic signals of a carboxyl group at δ_C 171.1 supporting the existence of an ester function (C-1). In addition, a signal of an *O*-bearing methylene carbon at δ_C 60.4 (C-1') was also notice and was in agreement the existence of the ester function. On the other hand, some characteristic signals of two terminal methyl groups at δ_C 19.7 (C-2) and 14.2 (C-51') together with a set aliphatic methylene carbons were observed at δ_C 21.1–31.1. The HMBC (Table 1, Fig. S3) spectrum reveals some important $^{2,3}J_{C\text{-}H}$ heteronuclear correlations which let us to position most of carbon atoms of our molecule. The correlation between the three protons appearing as a singlet at δ_H 1.98 with carbon atom C-1 (δ_C 171.1) was in agreement

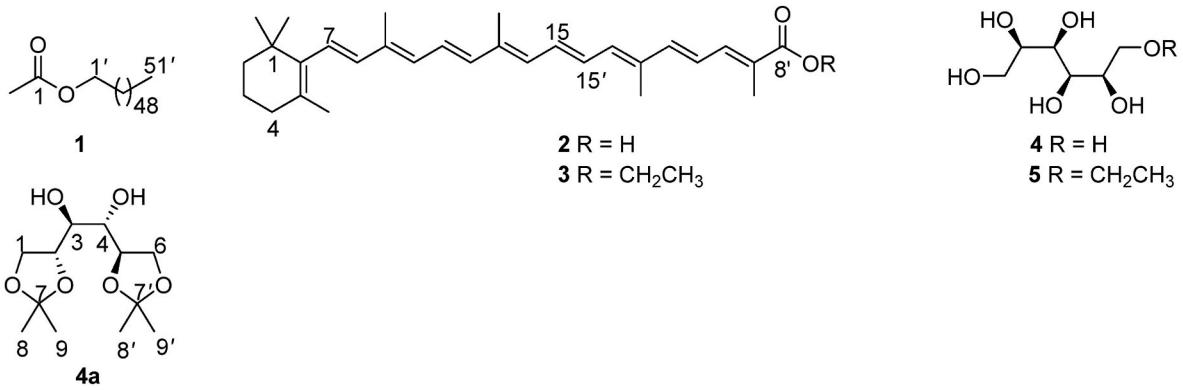

Fig. 1. Chemical structures of compound **1**–**5**.

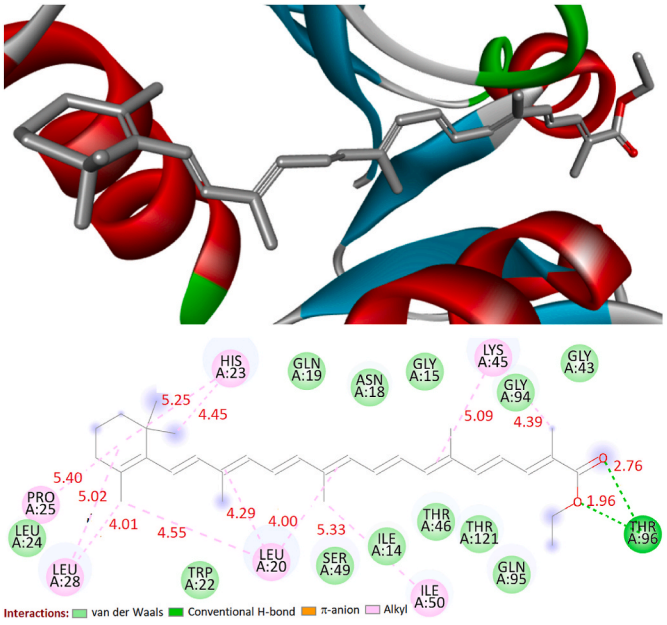

Fig. 2. The binding interactions of **2** against *S. aureus* (PDB: 2w9h).

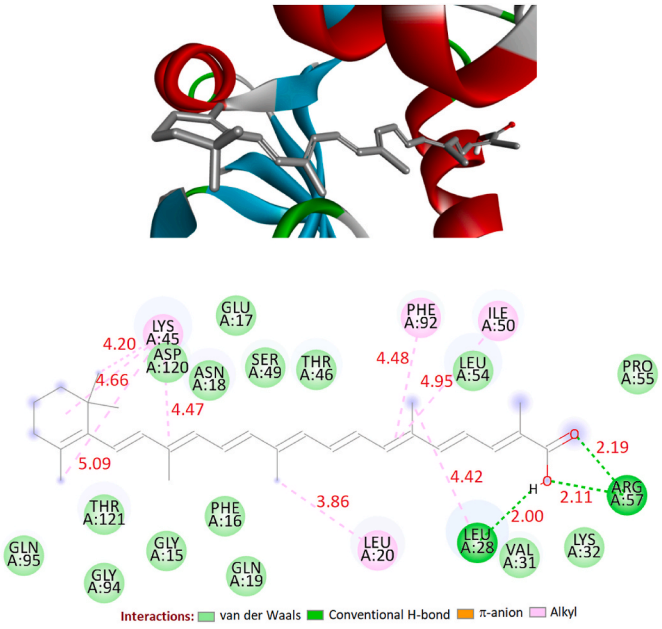

Fig. 3. The binding interactions of **3** against *S. aureus* (PDB: 2w9h).

with the existence of a methyl ester group in the structure of compound **1**. Moreover, the correlations between the proton H-51' (δ_H 0.85) with carbons C-50' (δ_C 22.6) and C-49' (δ_C 27.1) were also visible. Therefore, compound (**1**) was characterized as a new fatty ester derivative named henpentacontyl acetate.

Compound **3** was obtained as a yellow oil. Its ESI-TOF mass spectrum exhibited a *pseudo*-molecular ion peak at *m/z* 499.1 $[M+K]^+$ in agreement with the molecular formula $C_{32}H_{44}O_2K$ with 11 unsaturations. The MS spectrum also displayed characteristic fragments at *m/z* 393.3 $[M + K\text{-}106]^+$ due to the lost of toluene from the polyene chain and at *m/z* 416.4 $[M + H\text{-}C_2H_5O]^+$. The chemical shifts of this compound were identical to the corresponding data recorded for ethyl (all *E*)-8'-*trans*-apo-*β*-caroten-8'-oate from the literature [43–45].

Compound **2** was also obtained as a red amourphous powder. The ESI-TOF-MS in positive mode showed an $[M + Na]^+$ at *m/z* 455.3 (consistent with $C_{30}H_{40}O_2Na$) giving 11 unsaturations. The ^1H and ^{13}C NMR spectra were highly similar to those of compound ethyl (all *E*)-8'-*trans*-apo-*β*-caroten-8'-oate (**3**). Compound **2** differed from **3** by ^1H and ^{13}C NMR spectra indicating the absence of the ethyl ester group in favor of the carboxylic group characterized by the carbonyl at δ_C 170.3 (C-8') instead of δ_C 168.3 (C-8') for the ethyl ester. The ^{13}C NMR clearly shows the disappearance of the ethyl esters signals at 61.5 and δ_C 14.7. The complete analysis of 1D spectra in combination with data reported in the literature [46] [44]; allowed the identification of compound **2** as a carotenoid acid derivative namely *trans*-apo-8'-carotenoic acid.

Compound **4a** was synthesized from D-mannitol (**4**) using acetone in the presence of $ZnCl_2$ as catalyst and was obtained as white amorphous powder. The formation of diacetal is marked by the appearance on the ^{1}HNMR spectrum of signals at δ_H 1.25 and 1.29 integrating six protons each assigned to the four methyl groups of the two acetal rings. The ^{13}C NMR spectrum also shows three additional signals at δ_C 25.5, 26.8 and 108.1 affected to the carbons of the four methyl groups [C-8 (δ_C 25.4), C-8' (δ_C 25.4), C-9 (δ_C 26.8) and C-9' (δ_C 26.8)] and to two quaternary carbons of the acetal rings (C-7 et C-7'). In addition to these signals, the ^{1}HNMR spectrum also shows a doublet of two protons at δ_H 4.70 (2H, *d*, $J = 7.7$ Hz) attributed to the two hydroxyl groups OH-3 and OH-4, two split doublets of two protons each at δ_H 3.86 (2H, *dd*, $J = 8.2$; 5.0 Hz) and 3.96 (2H, *dd*, $J = 8.2$; 6.2 Hz) attributable to protons H_2-1 and H_2-6 respectively, a triplet at δ_H 3.43 (2H, *t*, $J = 8.0$ Hz, H-3; H-4) and a multiplet at δ_H 4.01 (2H, *m*). Comparison of the ^1H and ^{13}C NMR data of compound **4** with those of D-mannitol **4** indicated the disappearance of the hydroxyl signals in position 1, 2, 4 and 6 that usually appear on the proton spectrum of D-mannitol. The complete assignment of signals of the various protons and carbons was carried out using COSY, HSQC and HMBC spectra (Table S2).

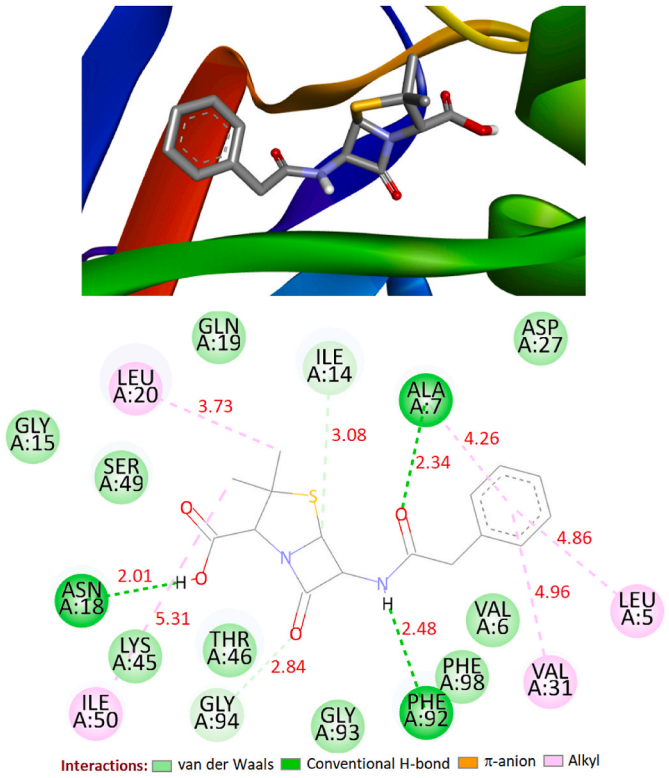

Fig. 4. The binding interactions of penicillin against *S. aureus* (PDB: 2w9h).

3.2. Physical aspects and spectroscopic data of compounds

Henpentacontyl acetate ***(1)****:* white solid, TOF-MS-ESI+: 792.6 $[M + NH_4]^+$ (calcd. *m/z* 792.9 for $C_{53}H_{106}O_2NH_4^+$). ^1H NMR ($CDCl_3$): δ_H 0.85 (3H, t, J = 6.7 Hz, 3H-51'), 1.15–1.25 [(CH_2)n, brs], 1.53 (2H, brs, 2H-2'), 1.98 (3H, s, 3H-2), 4.14 (2H, t, J = 6.7 Hz, 2H-1'). ^{13}C NMR ($CDCl_3$): δ_C 171.1 (C-1), 60.4 (C-1'), 21.1–31.1 (C-2'– C-50'), 19.7 (C-2) and 14.2 (C-51').

trans-apo-8′-carotenoic acid ***(2)****:* red solid. TOF-MS-ESI+: $[M+Na]^+$ at *m/z* = 455.3 for $C_{30}H_{40}O_2Na$. ^1H NMR ($CDCl_3$): δ_H 0.99 (6H, s, 2Me-1), 1.55 (2H, t, J = 5.5 Hz, H-3), 1.75 (2H, m, H-3), 1.77 (3H, s, Me-13'), 1.78 (3H, s, Me-13), 1.79 (3H, s, Me-9), 1.86 (3H, s, Me-5), 1.98 (3H, s, Me-9'), 2.14 (2H, t, J = 6.1 Hz, H-4), 6.33 (1H, d, H-14), 6.37 (2H, m, H-10/H-14'), 6.49 (2H, m, H-7/H-8), 6.51 (1H, d, J = 15.3 Hz, H-12), 6.57 (1H, m, H-15'), 6.62 (1H, m, H-12'), 6.63 (1H, m, H-15), 6.68 (1H, m, H-11'), 6.70 (1H, m, H-11), 7.29 (1H, m, H-10'). ^{13}C NMR (125 MHz, $CDCl_3$): δ_C 13.9 (Me-9'), 15.6 (Me-9), 16.0 (Me-13/Me-13'), 20.3 (C-3), 21.1 (Me-5), 28.9 (2Me-1), 33.8 (C-4), 34.9 (C-1), 38.6 (C-2), 128.3 (C-11), 128.6 (C-11'), 129.3 (C-7), 130.9 (C-9'), 131.0 (C-15/C-15'), 131.4 (C-10), 131.6 (C-5), 132.5 (C-14/C-14'), 135.8 (C-13/C-13'), 136.7 (C-12), 136.9 (C-8), 137.3 (C-9), 137.6 (C-6), 137.9 (C-10'), 138.5 (C-12'), 170.3 (C-8').

Ethyl-8′-trans-apo-β-caroten-8′-oate ***(3)****:* orange-yellow solid. TOF-MS-ESI+: $[M+K]^+$ at *m/z* = 499.1 for $C_{32}H_{44}O_2K$. ^1H NMR ($CDCl_3$): δ_H 1.00 (6H, s, 2Me-1), 1.37 (3H, t, $COOCH_2\underline{C}H_3$), 1.55 (2H, t, J = 5.5 Hz, H-3), 1.75 (2H, m, H-3), 1.77 (3H, s, Me-13'), 1.78 (3H, s, Me-13), 1.79 (3H, s, Me-9), 1.89 (3H, s, Me-5), 1.96 (3H, s, Me-9'), 2.14 (2H, t, J = 6.1 Hz, H-4), 4.22 (2H, t, J = 6.0 Hz, $COO\underline{C}H_2CH_3$), 6.29 (1H, d, J = 11.4 Hz, H-10), 6.33 (1H, d, H-14), 6.37(1H, d, J = 11.3 Hz, H-14'), 6.41 (1H, d, J = 16.2 Hz, H-7), 6.49 (1H, m, H-8), 6.50 (1H, d, J = 15.3 Hz, H-12), 6.57 (1H, m, H-15'), 6.62 (1H, m, H-12'), 6.63 (1H, m, H-15), 6.67 (1H, m, H-11'), 6.68 (1H, m, H-11), 7.29 (1H, m, H-10'). ^{13}C NMR (125 MHz, $CDCl_3$): δ_C 14.2 (Me-9'), 14.7 ($COOCH_2\underline{C}H_3$), 15.6 (Me-9), 16.0 (Me-13/Me-13'), 20.3 (C-3), 21.1 (Me-5), 28.9 (2Me-1), 33.8 (C-4), 34.9 (C-1), 38.6 (C-2), 61.5 ($COO\underline{C}H_2CH_3$), 128.3 (C-11), 128.6 (C-11'), 129.3 (C-

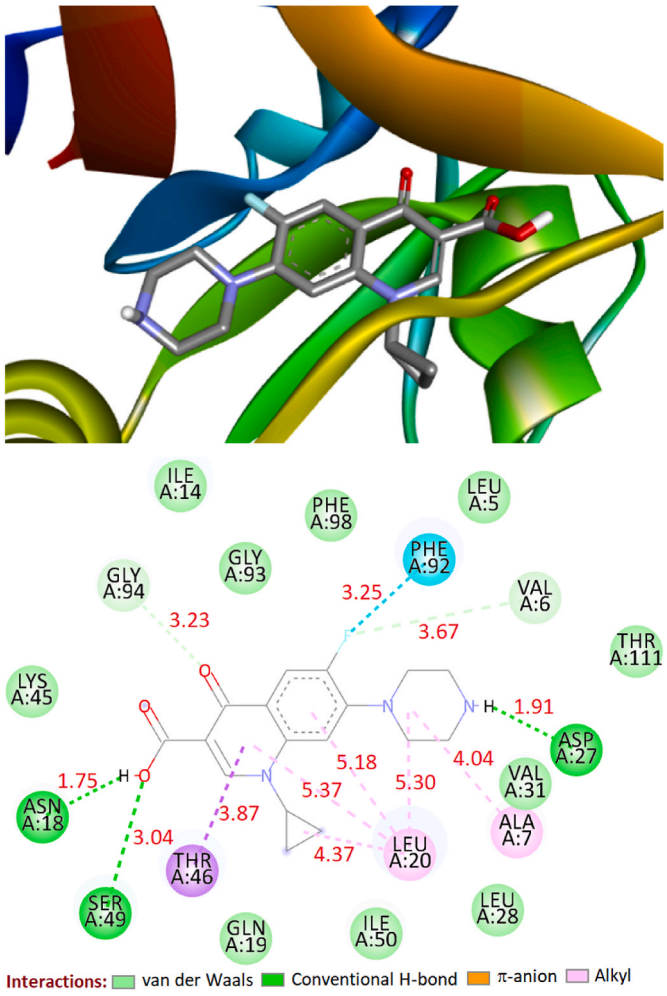

Fig. 5. The binding interactions of ciprofloxacin against *S. aureus* (PDB: 2w9h).

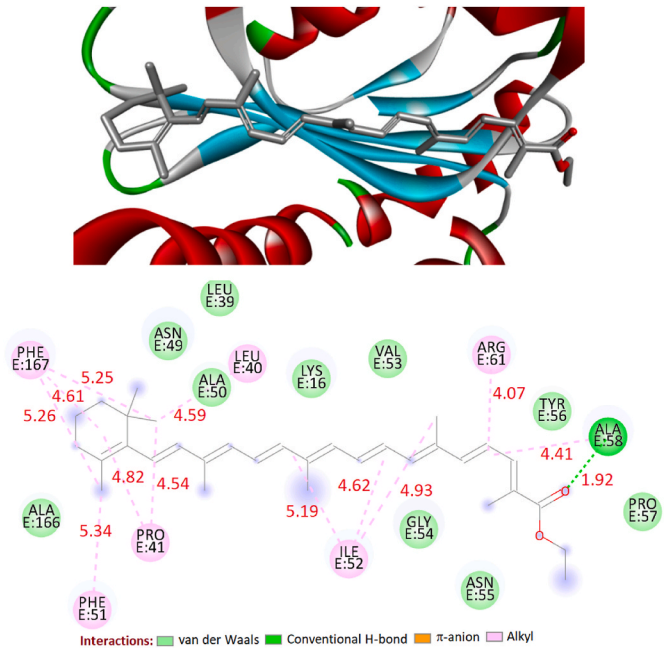

Fig. 6. The binding interactions of **2** against *P. aeruginosa LasR* (PDB: 2UV0).

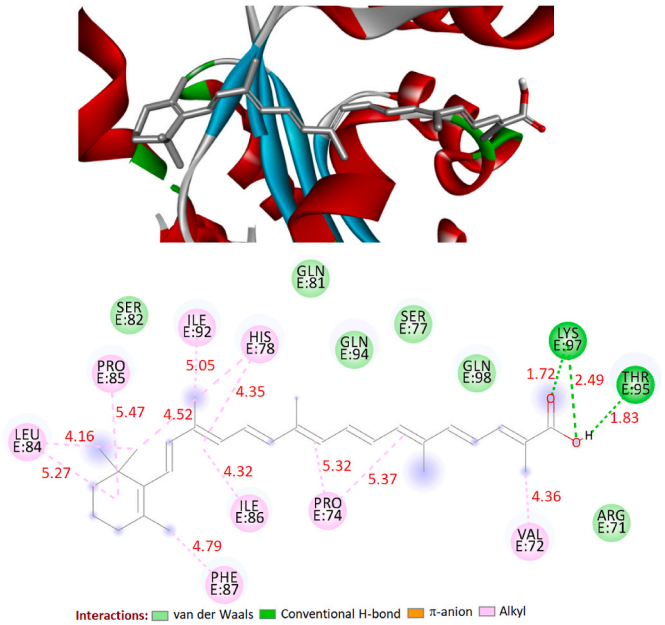

Fig. 7. The binding interactions of **3** against *P. aeruginosa LasR* (PDB: 2UV0).

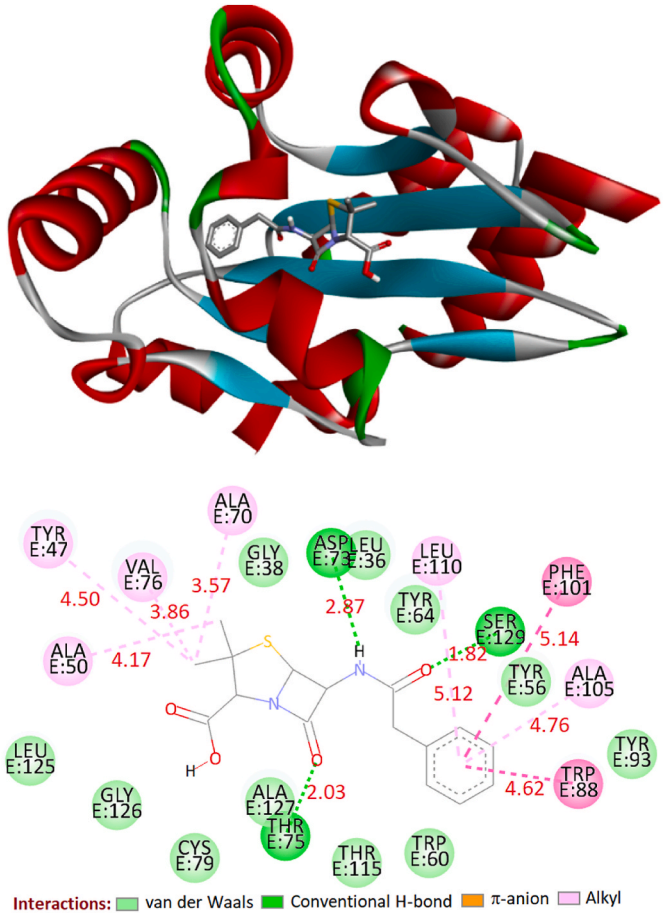

Fig. 8. The binding interactions of penicillin against *P. aeruginosa LasR* (PDB: 2UV0).

7), 130.8 (C-9'), 131.0 (C-15/C-15'), 131.4 (C-10), 131.6 (C-5), 132.5 (C-14/C-14'), 135.8 (C-13/C-13'), 136.7 (C-12), 136.9 (C-8), 137.3 (C-9), 137.6 (C-6), 138.5 (C-12'), 140.7 (C-10'), 168.3 (C-8').

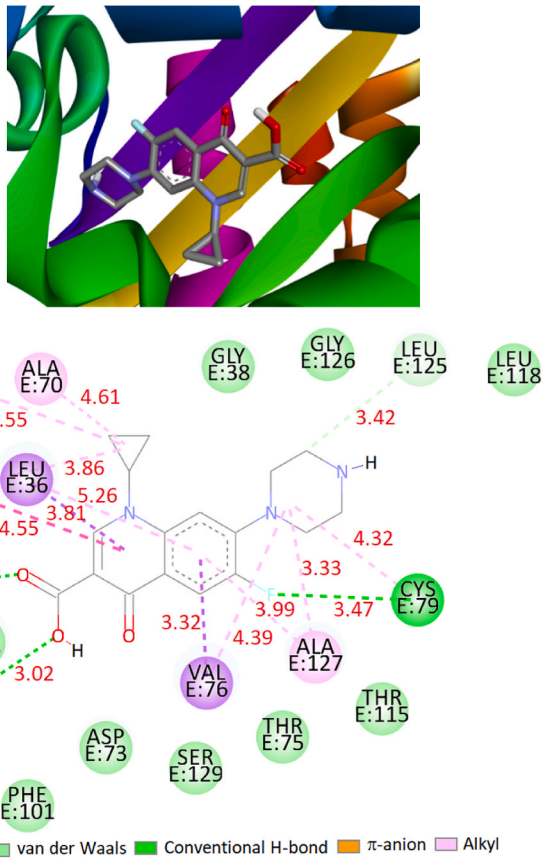

Fig. 9. The binding interactions of ciprofloxacin against *P. aeruginosa LasR* (PDB: 2UV0).

D-mannitol (4): white solid. ^{1}H NMR (DMSO-d_6): δ 4.41 (2H, d, J = 5.5 Hz, OH-2 and OH-5), 4.33 (2H, t, J = 5.7 Hz, OH-1 and OH-6), 4.13 (2H, d, J = 7.1 Hz, OH-3 and OH-4), 3.62 (2H, ddd, J = 10.8, 5.7, 3.5 Hz, H-1a and H-6a), 3.56 (2H, t, J = 7.5 Hz, H-3 and H-4), 3.47 (2H, m, H-2 and H-5) and 3.39 (2H, m, H-1b and H-6b). ^{13}C NMR (DMSO-d_6): δ_H 63.8 (C-1 and C-6), 71.3 (C-2 and C-5) and 69.7 (C-3 and C-4).

1,2:5,6-di-O-isopropylidene-D-mannitol ***(4a)****:* ^{1}H NMR (DMSO-d_6): δ_H 4.71 (2H, s, OH-3 and OH-4), 4.01 (2H, m, H-2 and H-5), 3.96 (2H, dd, J = 8.2; 6.2 Hz, H-1b and H-6b), 3.86 (2H, dd, J = 8.2; 5.0 Hz, H-1a and H-6a), 3.43 (2H, t, J = 8.0 Hz, H-3 and H-4), 1.25 (6H, s, 3H-8 and 3H-8'), 1.29 (6H, s, 3H-9 and 3H-9'). ^{13}C NMR (DMSO-d_6): 108.1 (C-7 and C-7') 74.8 (C-2 and C-5), 70.3 (C-3 and C-4), 66.6 (C-1 and C-6), 26.8 (C-9 and C-9') 25.4 (C-8 and C-8').

D-mannitol acetate ***(5)****:* white solid. TOF-MS-ESI+: $[M+Na]^+$ at m/z = 247.1 for $C_8H_{16}O_7Na$. ^{1}H NMR (DMSO-d_6): δ 4.75 (1H, d, J = 5.6 Hz, HO-2), 4.41 (1H, d, J = 5.5 Hz, HO-5), 4.33 (1H, t, J = 5.7 Hz, HO-6), 4.28 (2H, ov, H-1a and HO-3), 4.14 (2H, d, J = 7.1Hz, HO-4), 3.96 (1H, m, H-1b), 3.68 (1H, m, H-2), 3.62 (1H, m, H-6a), 3.54 (2H, m, H-3 and 4), 3.47 (1H, m, H-5) and 3.40 (1H, m, H-6b), 2.03 (3H, s, $OCOCH_3$). ^{13}C NMR (DMSO-d_6): δ_C 20.8 (-$OCOCH_3$), 63.8 (C-6), 67.0 (C-1), 68.2 (C-2), 69.3 (C-3), 69.4 (C-4), 71.2 (C-5) and 170.5 (-$OCOCH_3$).

3.3. Antimicrobial and molecular docking results

The antibacterial potential of compounds **1–5** were evaluated *in vitro* using microdilution method against seven clinically relevant bacterial strains including Gram-positive (*Staphylococcus aureus* ATCC700698, *Staphylococcus aureus* NR 46003) and Gram-negative (*Escherichia coli* ATCC25922, *Shigella Sonnei* NR519, *Pseudomonas aeruginosa* ATCC9721, *Salmonella. Typhi* ATCC6539, *Klebsiella pneumonia* NR41916) (Table 1). Ciprofloxacin served as the positive control. Following established

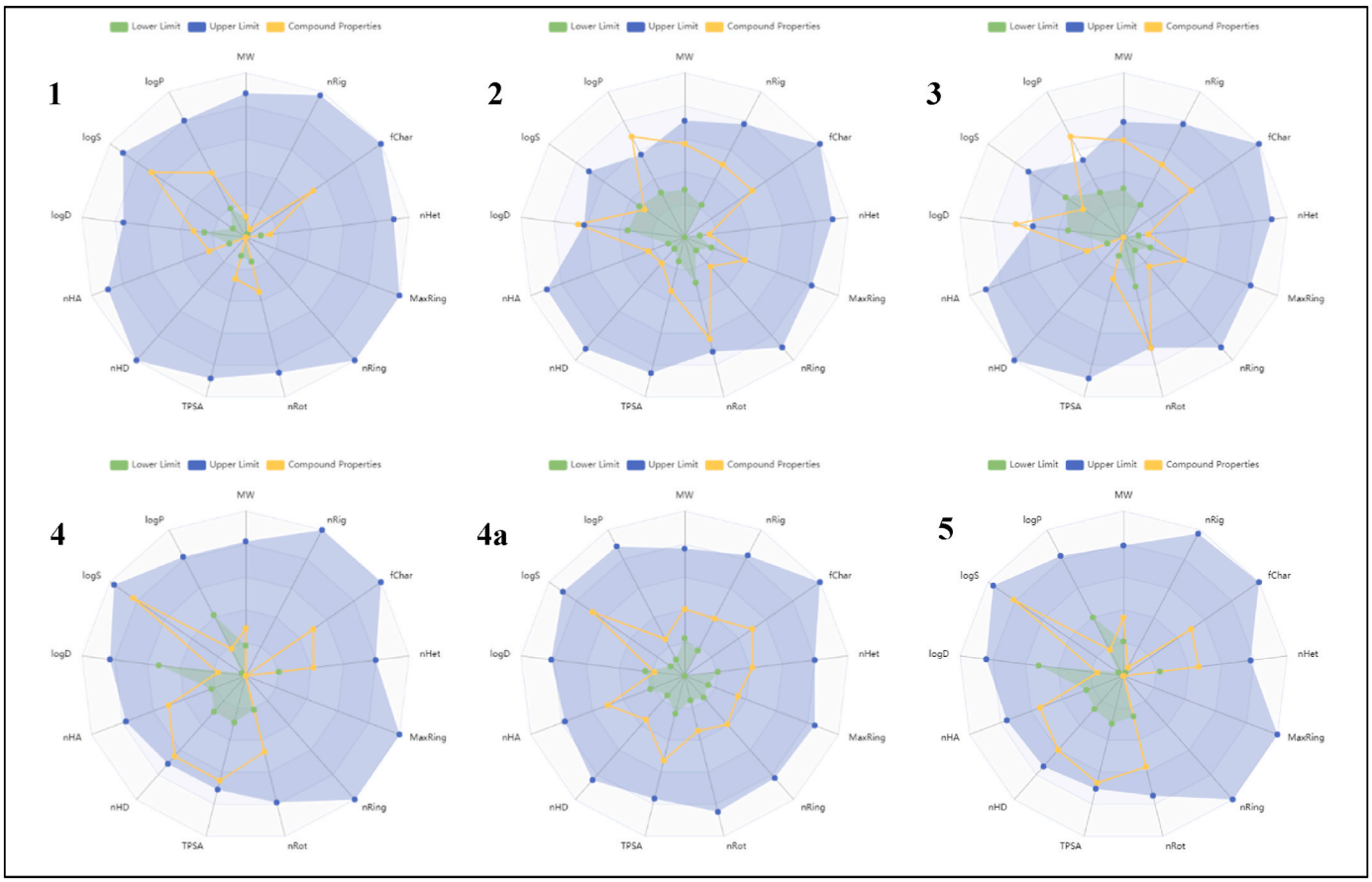

Fig. 10. Radar charts of compounds **1**–**5**.

Table 1
Antibacterial activity of isolated compounds.

Samples	Bacterial strains and MIC (μg/mL)						
	S. typhi ATCC6539	*S. aureus* ATCC700698	*S. aureus* NR46003	*E. coli* ATCC25922	*P. aeruginosa* ATCC9721	*S. Sonnei* NR519	*K. pneumonia* NR 41916
1	128	128	128	128	128	128	128
2	64	8	8	32	16	32	32
3	64	8	8	32	16	32	32
4	32	128	128	32	128	64	64
4a	>128	32	32	64	128	32	32
5	128	64	64	128	64	32	32
Cipro	1	2	0.250	0.125	1	0.250	4

Cipro = ciprofloxacin; Significant: MIC<10 μg/mL; Moderate: 10≤MIC<100 μg/mL; weak: 100≤MIC≤128 μg/mL MIC>128 μg/mL: inactive.

criteria [27,47], antibacterial activity was classified as significant (MIC <10 μg/mL), moderate (10 ≤ MIC <100 μg/mL), low (100 ≤ MIC ≤128 μg/mL), or inactive (MIC >128 μg/mL).

Compounds **2** and **3** exhibited significant antibacterial activity against both *S. aureus* strains (MIC = 8 μg/mL). Against other Gram-positive and Gram-negative strains, their activity were moderate ranging from 16 to 64 μg/mL. The remaining compounds (**1**, **4**, **5**) showed low to moderate activity depending on the bacterial strain. Notably, D-mannitol (**4**) displayed moderate activity against *S. typhi*, *E. coli*, *S. sonnei*, and *K. pneumoniae*, while its monoacetylated derivative, D-mannitol acetate (**5**), exhibited broader activity, particularly against both *S. aureus* strains, *P. aeruginosa*, *S. sonnei*, and *K. pneumoniae*. These observations suggest that acetylation of D-mannitol enhances lipophilicity and cell membrane penetration, improving antibacterial potency for several strains, consistent with prior reports that structural modification of polyols can increase bacterial uptake and bioactivity [48,49]. However, some exceptions were observed: *E. coli*, *P. aeruginosa*, and *S. typhi* were less susceptible to acetylated derivatives, highlighting species-specific differences in membrane permeability and efflux mechanisms. The fully protected derivative, 1,2:5,6-di-*O*-isopropylidene-D-mannitol (**4a**), was inactive against *S. typhi*, underscoring the importance of free hydroxyl groups for antibacterial action. The newly isolated henpentacontyl acetate (**1**) demonstrated weak activity, possibly due to its long aliphatic chain reducing solubility in aqueous media, consistent with previous studies showing that long-chain acetates often display limited diffusion across bacterial membranes [50]; [51].

To further probe the antibacterial potential, molecular docking was performed against *S. aureus* pyruvate kinase and *P. aeruginosa* targets, using ciprofloxacin and penicillin as positive controls (Table 2). Compounds **2** and **3** exhibited the highest binding affinities to *S. aureus* pyruvate kinase (−11.94 kcal/mol), exceeding those of ciprofloxacin (−8.54 kcal/mol) and penicillin (−8.16 kcal/mol). This suggests that the carboxylate moiety in compound **2** and the ester functionality in

Table 2
Molecular docking scores and the corresponding prominent residual amino acid interactions of the isolated compounds and standard drugs penicillin and ciprofloxacin against *S. aureus* and *P. aeruginosa LasR*.

	Lowest binding energy (kcal/mol)	K_i(μM)	Lowest binding energy (kcal/mol)	K_i (μM)
	Against *S. aureus* (PDB: 2w9h)		Against *P. aeruginosa LasR* (PDB: 2uv0)	
2	−11.94	0.002	−8.46	0.633
3	−11.74	0.003	−7.58	2.760
4	−3.97	1230.00	−3.79	1680.00
4a	−6.76	11.110	−6.70	12.280
5	−4.28	724.670	−4.21	814.640
Cipro	−8.54	0.553	−8.29	0.842
Peni	−8.16	1.050	−8.62	0.484

Peni = penicillin, Cipro = ciprofloxacin; K_i = inhibition constant.

compound **3** facilitate strong hydrogen bonding and hydrophobic interactions with the enzyme's active site. The *in silico* findings align with the *in vitro* MIC data, confirming that these apocarotenoid derivatives are promising antibacterial leads. Recent studies have similarly demonstrated that apocarotenoids and related plant-derived metabolites exhibit high docking scores against essential bacterial enzymes, correlating with observed MIC reductions [52–54] (see Table 3).

While specific docking values vary depending on target and software, contemporary studies on plant-derived antibacterial leads demonstrate similar docking affinities in the −9 to −12 kcal/mol range for potent hits [55]. The alignment of strong docking results with low MIC values strengthens the case for compounds **2** and **3** as true leads rather than artefacts of screening. When compared to recent research, these compounds fit within the emerging trend of plant-derived small molecules gaining relevance in the fight against AMR. For example, the 2023 systematic review highlighted that fewer than 10 % of reviewed plant compounds reached MIC <10 μg/mL, making the performance of **2** and **3** noteworthy [55]. Moreover, structural modification (e.g., acetylation, esterification) shown here for compounds **4** and **5** demonstrates that semi-synthetic manipulation remains a valuable strategy for enhancing antibacterial potency; such strategies are increasingly featured in recent literature [56].

Overall, the results indicate that structural modifications such as esterification or acetylation can modulate antibacterial activity, and that compounds **2** and **3** possess significant potential as natural antibacterial agents. These findings support the traditional use of *G. aqualla* for treating oral and ear infections and provide a basis for further *in vivo* evaluation and structure–activity relationship (SAR) studies.

3.4. ADMET study

Compound **1**, the smallest compound (MW = 102.07), has favorable permeability and reasonable oral bioavailability (F20 % = 0.102). It has a good balance of solubility and lipophilicity (logS = −0.661, logP = 1.224). Plasma protein binding is low, and it crosses the BBB well (0.833), indicating potential CNS effects. It shows limited metabolic interactions but slightly higher clearance (8.02) and shorter half-life (0.8 h). Toxicity is low in most categories, though eye irritation and genotoxic alerts are present. It is environmentally safer than most others. Overall, Compound **1** is a well-rounded candidate with moderate pharmacokinetics and low toxicity.

Compound **3** has a relatively high molecular weight (460.33 g/mol) and low aqueous solubility (logS = −6.118), indicating it is lipophilic (logP = 5.177) and potentially poorly soluble in water. Absorption is limited (low Caco-2 and MDCK permeability), and it has low bioavailability (<5 % at 20 % threshold). It binds strongly to plasma proteins (PPB = 94.81 %) and inhibits multiple transporters (e.g., OATP1B1, MRP1). Metabolically, it is a substrate and inhibitor for several CYP enzymes (CYP1A2, CYP2C9, CYP3A4), indicating a high risk of drug-drug interactions. Its clearance rate is high (8.99 mL/min/kg), but its half-life is short (0.26 h). Toxicity risk is moderate, with alerts for DILI, AMES mutagenicity, and hERG inhibition. Environmentally, it shows high bioconcentration potential. Similar to compound **3**, compound **2** has a high molecular weight (432.3 g/mol) and poor solubility (logS = −4.474). It is slightly more polar (TPSA = 37.3) and somewhat easier to synthesize (Synth = 3.0). Toxicity is again moderate, with risks for DILI and skin sensitization. Environmentally, it is similar to Compound **3** with high aquatic toxicity and bioconcentration factors.

Compound **4** is quite different it's much smaller (MW = 182.08) and highly polar (TPSA = 121.38), with good aqueous solubility (logS = −0.172) and zero logP, making it very hydrophilic. It has no medicinal chemistry alerts, but absorption is very poor due to low permeability (Caco-2 = −6.2). It is minimally bound to plasma proteins (PPB = 27.39 %) and is not a significant substrate or inhibitor of transporters. It avoids most CYP interactions, making it metabolically stable. Its clearance is low, but half-life is longer (1.77 h).

Compound **4a** is a derivative of Compound 3 with slightly higher molecular weight and lower polarity. It has better drug-likeness (QED = 0.746) and a good synthetic profile. While permeability improves slightly, oral bioavailability remains poor (F20 % = 0.029). It has low plasma protein binding (PPB = 17.95 %), but better blood-brain barrier penetration (BBB = 0.756), suggesting potential CNS effects. It does not significantly inhibit or act as a substrate for major CYPs, which supports metabolic safety. The half-life is the longest among all compounds (3.32 h), showing potential for extended dosing intervals.

Compound **5** is a moderately sized compound (MW = 224.09) with high polarity (TPSA = 127.45), indicating good solubility (logS = −0.233). However, absorption remains low (HIA = 0.053), and Pgp interaction is notable. It binds weakly to plasma proteins and shows poor metabolic interactions an advantage. Environmentally, it shows moderate aquatic toxicity but low bioaccumulation.

The radar charts provide a visual comparison of key physicochemical properties for compounds **1** through **5** and **4a** against acceptable drug-likeness boundaries (green and blue shaded areas). Compound **3** stands out for aligning most closely within the ideal property space, suggesting strong drug-likeness and balanced attributes across parameters like logP, MW, TPSA, and H-bonding features. Compound **4a** also demonstrates a well-rounded profile with favorable improvements in molecular weight, polarity, and synthetic accessibility. Compounds **4** and **5** show strong alignment in polarity-related properties (TPSA and solubility), indicating hydrophilicity and potential metabolic safety. Compounds **2** and **3**, although more lipophilic and larger in size, show consistent patterns in molecular complexity and ring systems, indicating structural robustness. Overall, the radar plots highlight the strengths of each compound's profile, with Compounds **1** and **4a** displaying the most favorable balance for further development.

In silico ADMET and drug-likeness predictions suggest that compounds **2** and **3** have acceptable predicted human intestinal absorption, moderate predicted clearance, and no obvious major hepatotoxicity flags within the modelling limits. Their dual demonstration of strong binding, low MIC, and acceptable predicted pharmacokinetics strengthens the case to progress into preclinical development. These findings support further exploration of these leads. The broader literature indicates that plant-derived antibacterials often fail at the ADMET/drug-likeness stage [55,57], so the favorable predicted profile here is encouraging.

The significant antibacterial activities of compounds **2** and **3** from *G. aqualla*, combined with favorable docking and ADMET predictions, reflect a paradigm increasingly seen in recent studies of natural products. For instance, Prinsa et al. [23] showed that careful structural and computational profiling of flavonoids can yield strong lead-molecules with quantifiable binding affinities and predicted drug-likeness. Furthermore, the semi-synthetic modification strategies reported by Karim et al. [58] underline that small chemical changes (e.g., esterification, acetylation) can meaningfully enhance potency, as we observed

Table 3
Drug-likeness prediction and ADMET properties of compounds **1**–**5**.

Physicochemical Property						
Property	1	2	3	4	4a	5
Molecular Weight	102.07	432.3	460.33	182.08	262.14	224.09
Volume	109.98	510.095	544.687	165.074	251.737	205.819
Density	0.928	0.847	0.845	1.103	1.041	1.089
nHA	2.0	2.0	2.0	6.0	6.0	7.0
nHD	0.0	1.0	0.0	6.0	2.0	5.0
nRot	3.0	9.0	11.0	5.0	3.0	7.0
nRing	0.0	1.0	1.0	0.0	2.0	0.0
MaxRing	0.0	6.0	6.0	0.0	5.0	0.0
nHet	2.0	2.0	2.0	6.0	6.0	7.0
fChar	0.0	0.0	0.0	0.0	0.0	0.0
nRig	1.0	15.0	15.0	0.0	10.0	1.0
Flexibility	3.0	0.6	0.733	0.0	0.3	7.0
Stereo Centers	0.0	0.0	0.0	4.0	4.0	4.0
TPSA	26.3	37.3	26.3	121.38	77.38	127.45
logS	−0.661	−4.474	−6.118	−0.172	−0.723	−0.233
logP	1.224	4.417	5.177	−1.736	0.542	−1.579
logD	1.269	3.274	3.979	−1.413	0.803	−1.241
pka (Acid)	10.955	5.969	10.197	7.987	10.645	7.123
pka (Base)	5.524	3.775	6.149	3.957	5.481	3.17
Melting point	−95.051	187.127	142.223	159.024	94.341	129.011
Boiling point	99.483	331.327	355.617	325.025	189.125	301.227
Medicinal Chemistry						
QED	0.485	0.292	0.185	0.261	0.746	0.304
GASA	0.0	0.0	0.0	0.0	0.0	0.0
Synth	1.0	3.0	3.0	3.0	4.0	3.0
Fsp3	0.8	0.367	0.406	1.0	1.0	0.875
MCE-18	0.0	15.537	15.311	4.0	40.0	5.0
NPscore	0.472	1.793	1.566	1.143	0.914	1.664
Lipinski Rule	0.0	0.0	0.0	0.0	0.0	0.0
Pfizer Rule	0.0	1.0	1.0	0.0	0.0	0.0
GSK Rule	0.0	1.0	1.0	0.0	0.0	0.0
Golden Triangle	1.0	0.0	0.0	1.0	0.0	0.0
PAINS	0 alerts	0 alerts	0 alerts	0 alerts	0 alerts	0 alerts
ALARM NMR	0 alerts	0 alerts	1 alerts	0 alerts	0 alerts	0 alerts
BMS	0 alerts	1 alerts	1 alerts	0 alerts	0 alerts	0 alerts
Chelator Rule	0 alerts	0 alerts	0 alerts	0 alerts	0 alerts	0 alerts
Colloidal aggregators	0.02	0.994	0.999	0.018	0.233	0.161
FLuc inhibitors	0.0	0.666	0.653	0.0	0.0	0.0
Blue fluorescence	0.006	0.008	0.013	0.024	0.035	0.037
Green fluorescence	0.0	0.042	0.056	0.0	0.0	0.0
Reactive compounds	1.0	0.68	0.695	0.585	0.668	0.502
Promiscuous compounds	0.183	0.203	0.115	0.158	0.047	0.219
Absorption						
Caco-2 Permeability	−4.413	−4.919	−4.918	−6.201	−4.971	−5.409
MDCK Permeability	−4.555	−4.748	−4.737	−3.915	−4.846	−4.194
PAMPA	0.262	0.989	0.222	1.0	0.836	0.999
Pgp-inhibitor	0.272	0.001	0.317	0.0	0.014	0.0
Pgp-substrate	0.457	0.766	0.228	0.285	0.573	0.59
HIA	0.036	0.0	0.0	0.135	0.035	0.053
F20 %	0.102	0.026	0.041	0.125	0.029	0.232
F30 %	0.158	0.124	0.302	0.142	0.061	0.581
F50 %	0.203	0.991	0.988	0.793	0.314	0.855
Distribution						
PPB	15.937	95.467	94.813	27.392	17.945	22.714
VDss	−0.094	0.095	0.495	−0.478	−0.286	−0.529
BBB	0.833	0.0	0.0	0.033	0.756	0.012
Fu	79.603	5.485	5.378	81.846	78.577	83.658
OATP1B1 inhibitor	0.471	1.0	0.999	0.957	0.407	0.99
OATP1B3 inhibitor	0.537	0.498	0.816	0.963	0.499	0.983
BCRP inhibitor	0.201	0.001	0.003	0.038	0.121	0.026
MRP1 inhibitor	0.901	0.946	0.972	0.022	0.56	0.12
Metabolism						
CYP1A2 inhibitor	0.151	0.0	0.659	0.056	0.0	0.009
CYP1A2 substrate	0.108	1.0	1.0	0.0	0.0	0.0
CYP2C19 inhibitor	0.245	0.095	1.0	0.0	0.0	0.001
CYP2C19 substrate	0.114	0.698	0.957	0.0	0.005	0.0
CYP2C9 inhibitor	0.045	0.004	0.529	0.069	0.005	0.027
CYP2C9 substrate	0.116	1.0	0.998	0.965	0.017	0.532
CYP2D6 inhibitor	0.15	0.001	0.402	0.0	0.004	0.039
CYP2D6 substrate	0.016	0.633	0.285	0.0	0.0	0.0
CYP3A4 inhibitor	0.127	0.001	0.733	0.0	0.0	0.0
CYP3A4 substrate	0.217	0.74	0.976	0.0	0.0	0.0
CYP2B6 inhibitor	0.129	0.992	1.0	0.204	0.038	0.022

(*continued on next page*)

Table 3 (*continued*)

Physicochemical Property						
Property	1	2	3	4	4a	5
CYP2B6 substrate	0.283	0.996	1.0	0.0	0.0	0.0
CYP2C8 inhibitor	0.984	0.999	1.0	0.925	0.503	0.96
HLM Stability	0.918	0.293	0.999	0.004	0.16	0.43
Excretion						
CL plasma	8.018	3.176	8.988	3.023	7.431	2.83
$T_{1/2}$	0.8	0.909	0.26	1.773	3.323	1.632
Toxicity						
hERG Blockers	0.079	0.054	0.152	0.008	0.008	0.007
hERG Blockers (10 μm)	0.59	0.128	0.538	0.04	0.308	0.04
DILI	0.232	0.74	0.464	0.003	0.827	0.013
AMES Mutagenicity	0.112	0.366	0.438	0.559	0.829	0.689
Rat Oral Acute Toxicity	0.06	0.632	0.583	0.004	0.682	0.004
FDAMDD	0.054	0.67	0.872	0.003	0.004	0.005
Skin Sensitization	0.711	0.782	0.794	0.836	0.496	0.881
Carcinogenicity	0.613	0.656	0.697	0.183	0.987	0.234
Eye corrosion	0.987	0.027	0.014	0.001	0.184	0.002
Eye irritation	0.998	0.747	0.674	0.664	0.963	0.627
Respiratory	0.195	0.79	0.748	0.002	0.491	0.002
Human Hepatotoxicity	0.086	0.615	0.504	0.374	0.88	0.348
Drug-induced Nephrotoxicity	0.062	0.859	0.643	0.253	0.003	0.228
Ototoxicity	0.128	0.733	0.547	0.974	0.814	0.943
Hematotoxicity	0.121	0.516	0.307	0.089	0.012	0.122
Genotoxicity	0.001	0.599	0.387	0.001	0.003	0.01
RPMI-8226 Immunitoxicity	0.028	0.049	0.08	0.038	0.001	0.034
A549 Cytotoxicity	0.006	0.016	0.075	0.012	0.007	0.008
Hek293 Cytotoxicity	0.027	0.127	0.403	0.016	0.297	0.014
Drug-induced Neurotoxicity	0.075	0.324	0.453	0.003	0.001	0.006
Environmental toxicity						
Bioconcentration Factors	0.223	2.059	2.967	0.105	0.173	0.138
IGC50	1.87	4.663	5.062	1.089	1.767	1.64
LC_{50} FM	3.233	5.499	6.318	1.206	2.169	2.466
LC_{50} DM	2.803	5.756	6.25	1.855	2.813	2.838
Tox21 pathway						
NR-AhR	0.0	0.0	0.002	0.0	0.004	0.0
NR-AR	0.0	0.005	0.006	0.0	0.039	0.0
NR-AR-LBD	0.0	0.0	0.0	0.0	0.001	0.0
NR-Aromatase	0.0	0.993	0.999	0.0	0.008	0.0
NR-ER	0.034	0.196	0.447	0.004	0.074	0.007
NR-ER-LBD	0.0	0.704	0.924	0.0	0.003	0.0
NR-PPAR-gamma	0.0	0.811	0.32	0.0	0.0	0.0
SR-ARE	0.0	0.998	0.999	0.0	0.043	0.0
SR-ATAD5	0.0	0.181	0.176	0.0	0.003	0.0
SR-HSE	0.0	0.993	0.996	0.0	0.001	0.0
SR-MMP	0.0	0.995	0.999	0.0	0.004	0.0
SR-p53	0.0	0.02	0.041	0.0	0.004	0.0
Toxicophore Rules						
Acute Toxicity Rule	0	0	0	0	0	0
Genotoxic Carcinogenicity Rule	0	0	1 alerts	0	0	0
NonGenotoxic Carcinogenicity Rule	0	0	0	0	0	0
Skin Sensitization Rule	0	1 alerts	2 alerts	0	1 alerts	0
Aquatic Toxicity Rule	0	2 alerts	3 alerts	1 alerts	1 alerts	1 alerts
NonBiodegradable Rule	0	0	0	0	1 alerts	0
SureChEMBL Rule	0	2 alerts	2 alerts	0	0	0
FAF-Drugs4 Rule	0	2 alerts	2 alerts	0	0	0

in our D-mannitol derivatives. These parallels suggest that our findings not only validate the ethnobotanical use of *G. aqualla* but also position our compounds within the cutting-edge framework of natural product antimicrobial research. Going forward, the convergence of micro-dilution screening, docking, and ADMET modelling will be critical for advancing these leads toward translational development.

4. Conclusion

Phytochemical investigation of the methanolic extract of *Gardenia aqualla* stem bark resulted in the isolation of a new ester, henpentacontyl acetate (**1**), along with four known compounds (**2**–**5**). Among these, compounds **2** and **3** exhibited significant antibacterial activity against *Staphylococcus aureus* ATCC700698 and *S. aureus* NR46003 (MIC = 8 μg/mL), while the remaining compounds showed weak to moderate activity against other tested Gram-positive and Gram-negative bacteria. Molecular docking analysis against *S. aureus* pyruvate kinase revealed that compounds **2** and **3** possessed higher binding affinities (−11.94 kcal/mol) than ciprofloxacin (−8.54 kcal/mol) and penicillin (−8.16 kcal/mol), supporting their potential as lead scaffolds for antibacterial drug development. ADMET predictions further indicated that these compounds display favorable pharmacokinetic and safety profiles, with compound **1** showing good permeability and low toxicity, and the D-mannitol derivative (**4a**) demonstrating enhanced drug-likeness, metabolic stability, and blood–brain barrier penetration. Collectively, these findings provide scientific evidence for the traditional use of *G. aqualla* in managing bacterial infections and highlight compounds **2**, **3**, and **4a** as promising candidates for further development of antibacterial agents targeting *S. aureus* and possibly other pathogenic bacteria.

CRediT authorship contribution statement

Jean Noël Nyemb: Writing – review & editing, Supervision, Project administration, Data curation, Conceptualization. **Gaetan Bayiha Ba Njock:** Writing – original draft, Software, Methodology, Investigation, Formal analysis, Data curation. **Taye B. Demissie:** Writing – original draft, Software, Methodology, Investigation, Formal analysis, Data curation. **Japheth O. Ombito:** Writing – original draft, Software, Methodology, Investigation, Formal analysis, Data curation. **Syeda Abida Ejaz:** Writing – original draft, Software, Methodology, Investigation, Formal analysis, Data curation. **Hafiz Muhammad Attaullah:** Writing – original draft, Software, Funding acquisition, Formal analysis, Data curation. **Céline Henoumont:** Writing – original draft, Software, Methodology, Investigation, Formal analysis, Data curation. **Sophie Laurent:** Writing – original draft, Software, Methodology, Investigation, Formal analysis, Data curation. **Alembert Tiabou Tchinda:** Writing – original draft, Software, Methodology, Investigation, Formal analysis, Data curation. **Emmanuel Talla:** Writing – original draft, Software, Methodology, Investigation, Formal analysis, Data curation. **Marcello Iriti:** Writing – review & editing, Supervision, Methodology, Investigation, Conceptualization.

Declaration of competing interest

The authors declare that they have no known competing financial interests or personal relationships that could have appeared to influence the work reported in this paper.

Appendix A. Supplementary data

Supplementary data to this article can be found online at https://doi.org/10.1016/j.micpath.2025.108182.

Data availability

Data will be made available on request.

References

[1] Antimicrobial Resistance Collaborators, Global burden of bacterial antimicrobial resistance in 2019: a systematic analysis, Lancet 399 (10325) (2022) 629–655, https://doi.org/10.1016/S0140-6736(21)02724-0.

[2] J. O'neill, Review on antimicrobial resistance, in: Antimicrobial Resistance: Tackling a Crisis for the Health and Wealth of Nations, vol. 20p, 2014.

[3] J. O'Neill, Tackling drug-resistant Infections Globally: Final Report and Recommendations. Review on Antimicrobial Resistance, Wellcome Trust and HM Government, 2016, p. 84p.

[4] D.J. Newman, G.M. Cragg, Natural products as sources of new drugs over the last 25 years, J. Nat. Prod. 70 (3) (2007) 461–477.

[5] D.J. Newman, G.M. Cragg, Natural products as sources of new drugs over the 30 years from 1981 to 2010, J. Nat. Prod. 75 (3) (2012) 311–335.

[6] D.J. Newman, G.M. Cragg, Natural products as sources of new drugs from 1981 to 2014, J. Nat. Prod. 79 (3) (2016) 629–661.

[7] D.J. Newman, G.M. Cragg, Natural products as sources of new drugs over the nearly four decades from 01/1981 to 09/2019, J. Nat. Prod. 83 (3) (2020) 770–803.

[8] D.J. Newman, G.M. Cragg, K.M. Snader, Natural products as sources of new drugs over the period 1981– 2002, J. Nat. Prod. 66 (7) (2003) 1022–1037.

[9] D. Bernard, Y. Hassana, M. Djaouda, M. Mathieu, W.B. Romeo, K. Benoît, A. T. Wahab, Antibacterial effects of a new triterpenoid saponin from roots of *Gardenia ternifolia* Schumach. & Thonn (Rubiaceae), Results Chem. 4 (2022) 100366.

[10] J.N. Nyemb, L.M. Magnibou, E. Talla, A.T. Tchinda, R.T. Tchuenguem, C. Henoumont, J.T. Mbafor, Lipids constituents from *Gardenia aqualla* stapf & hutch, Open Chem. 16 (1) (2018) 371–376.

[11] D. Martins, C.V. Nunez, Secondary metabolites from Rubiaceae species, Molecules 20 (7) (2015) 13422–13495.

[12] S. Mongrand, A. Badoc, B. Patouille, C. Lacomblez, M. Chavent, J.-J. Bessoule, Chemotaxonomy of the Rubiaceae family based on leaf fatty acid composition, Phytochemistry (Elsevier) 66 (5) (2005) 549–559.

[13] C.G. Pereira, M.A.A. Meireles, Supercritical fluid extraction of bioactive compounds: fundamentals, applications and economic perspectives, Food Bioprocess Technol. 3 (2010) 340–372.

[14] POWO, Plants of the World Online, Facilitated by the Royal Botanic Gardens, Kew, 2023. Published on the Internet. Retrieved September 14, 2023, http://www.plantsoftheworldonline.org/.

[15] N. Rakotonirina, B. Rakouth, A.P. Davis, A taxonomic revision of Madagascan *Gardenia* (Rubiaceae, Gardenieae), Nord. J. Bot. 30 (6) (2012) 712–728.

[16] S.M. Mohamed, S.A. Ross, M.A.M. Ahmed, Diverse glycosides from *Gardenia latifolia* with antiviral activity and chemosystematic significance, Rev. Bras. Farmacogn. 32 (2022) 1038–1041, https://doi.org/10.1007/s43450-022-00335-w.

[17] J.N. Nyemb, R.T. Tchuenguem, A. Venditti, A.T. Tchinda, C. Henoumont, E. Talla, J. Iqbal, Antimicrobial and α-glucosidase inhibitory activities of chemical constituents from *Gardenia aqualla* (Rubiaceae), J. Nat. Prod. 36 (24) (2022) 6369–6374, https://doi.org/10.1080/14786419.2022.2031187.

[18] H.M. Burkill, The Useful Plants of West Tropical Africa, vol. 1, Families A-D: Royal Botanic Gardens, 1985.

[19] H.M. Burkill, The Useful Plants of West Tropical Africa. Volume 4: Families M-R, Royal Botanic Gardens, 1997.

[20] C.B. Ngalemo, G.L. Tchiengang Tchoua, F.N. Bony, B.G. Tsawo, P.Y. Mbopi, et al., Polyphenolic and flavonoids contents and antibacterial activity of hydro-ethanolic and aqueous extract of fresh leaves of *Gardenia aqualla*, Int. J. Pharm. Chem. 8 (6) (2023) 75–81, https://doi.org/10.11648/j.ijpc.20220806.12.

[21] M. Kara, N. Haoudi, N.E.H. Tahiri, F.Z. Rhebbar, R.E. Mernissi, A. Assouguem, H. Slali, J. Bahhou, Chemical profiling, antioxidant and antimicrobial activities, and *in silico* evaluation of *Gardenia jasminoides* essential oil, Plants 14 (7) (2025) 1055, https://doi.org/10.3390/plants14071055.

[22] Y. Zhu, A comparative study on antimicrobial effects of Rubiaceae plants, Theor. Nat. Sci. 48 (2024) 118–123.

[23] Supriyo Saha S. Prinsa, Md Z.H. Bulbul, Y. Yasuhiro Ozeki, A. Mubarak, M. A. Alamri, S.M.A. Kawsar, Flavonoids as potential KRAS inhibitors: DFT, molecular docking, molecular dynamics simulation and ADMET analyses, J. Asian Nat. Prod. Res. 26 (8) (2024) 955–992, https://doi.org/10.1080/10286020.2024.2343821.

[24] S.T. Quayum, N.J.I. Esha, S. Siraji, S.S. Al Abbad, Z.H.A. Alsunaidi, M. H. Almatarneh, S. Shofiur Rahman, A.N. Alodhayb, K.A. Alibrahim, S.M.A. Kawsar, K.M. Uddin, Exploring the effectiveness of flavone derivatives for treating liver diseases: utilizing DFT, molecular docking, and molecular dynamics techniques, MethodsX 12 (2024) 102537, https://doi.org/10.1016/j.mex.2023.102537, 2024.

[25] E. de Alvarenga, V.S.F.O. Carneiro, W. Saliba, A high yield synthesis of 1,2: 5,6-di-*O*-isopropylidene-D-mannitol, J. Chil. Chem. Soc. 51 (3) (2006) 986–988.

[26] J.J. Farmer, Enterobacteriaceae: introduction and identification, in: P.R. Murray, E.J. Baron, M.A. Pfaller, F.C. Tenover, R.H. Yolken (Eds.), Manual of Clinical Microbiology, sixth ed., American Society for Microbiology, Washington DC, 1995, pp. 438–449.

[27] J.N. Nyemb, T.A. Tchinda, E. Talla, E.B. Nanga, T.D. Ngoudjou, C. Henoumont, S. Laurent, J. Iqbal, T. Joseph, J.T. Mbafor, Vitellaroside, a new cerebroside from *Vitellaria paradoxa* (Sapotaceae) and its bioactivities, Nat. Prod. Chem. Res. 6 (2018) 306.

[28] A.R. Allouche, Gabedit—A graphical user interface for computational chemistry softwares, J. Comput. Chem. 32 (1) (2011) 174–182.

[29] M.J. Bottomley, E. Muraglia, R. Bazzo, A. Carfì, Molecular insights into quorum sensing in the human pathogen *Pseudomonas aeruginosa* from the structure of the virulence regulator LasR bound to its autoinducer, JBC 282 (18) (2007) 13592–13600, https://doi.org/10.1074/jbc.M700556200.

[30] H. Heaslet, M. Harris, K. Fahnoe, R. Sarver, H. Putz, J. Chang, C. Subramanyam, G. Barreiro, J.R. Miller, Structural comparison of chromosomal and exogenous dihydrofolate reductase from *Staphylococcus aureus* in complex with the potent inhibitor trimethoprim, Proteins 76 (3) (2009) 706–717, https://doi.org/10.1002/prot.22383.

[31] M. Bitew, T. Desalegn, T.B. Demissie, A. Belayneh, M. Endale, R. Eswaramoorthy, Pharmacokinetics and drug-likeness of antidiabetic flavonoids: molecular docking and DFT study, PLoS One 16 (12) (2021) e0260853.

[32] T. Damena, M.B. Alem, D. Zeleke, T. Desalegn, R. Eswaramoorthy, T.B. Demissie, Novel zinc (II) and copper (II) complexes of 2-((2-Hydroxyethyl) amino) quinoline-3-carbaldehyde for antibacterial and antioxidant activities: a combined experimental, DFT, and docking studies, ACS Omega 7 (30) (2022) 26336–26352, https://doi.org/10.1021/acsomega.2c02205.

[33] F. Lemilemu, M. Bitew, T.B. Demissie, R. Eswaramoorthy, M. Endale, Synthesis, antibacterial and antioxidant activities of Thiazole-based Schiff base derivatives: a combined experimental and computational study, BMC Chem 15 (1) (2021) 1–18.

[34] A.D. Becke, Density-functional thermochemistry. V. Systematic optimization of exchange-correlation functionals, J. Chem. Phys. 107 (20) (1997) 8554–8560.

[35] C. Lee, W. Yang, R.G. Parr, Development of the Colle-Salvetti correlation-energy formula into a functional of the electron density, Phys. Rev. B 37 (2) (1988) 785.

[36] H.D. T Jr., Gaussian basis sets for use in correlated molecular calculations. I. The atoms boron through neon and hydrogen, J. Chem. Phys. 90 (2) (1989) 1007–1023, https://doi.org/10.1063/1.456153.

[37] M.J. Frisch, G.W. Trucks, H.B. Schlegel, G.E. Scuseria, M.A. Robb, J.R. Cheeseman, J.A. Pople, Gaussian 16 (Version Revision C.01), Gaussian, Inc, Wallingford CT, 2016.

[38] G.M. Morris, D.S. Goodsell, R.S. Halliday, R. Huey, W.E. Hart, R.K. Belew, A. J. Olson, Automated docking using a Lamarckian genetic algorithm and an empirical binding free energy function, J. Comput. Chem. 19 (14) (1998) 1639–1662, https://doi.org/10.1002/(SICI)1096-987X(19981115)19:14<1639::AID-JCC10>3.0.CO;2-B.

[39] R. Ördög, V. Grolmusz, Evaluating genetic algorithms in protein-ligand docking. Paper Presented at the International Symposium on Bioinformatics Research and Applications, 2008.

[40] C.T. Djoko, J.N. Nyemb, P. Sakava, A.Y. Gbaweng, S.A. Ejaz, R. Kanwal, Ba Njock G. Bayiha, J.D. Djithe, R.T. Feunaing, A. Venditti, E. Talla, Molecular docking and *in silico* ADMET evaluation of compounds from *Erythrina senegalensis*, as potential α-glucosidase and α-amylase inhibitors for the treatment of diabetes mellitus, J. Phytomol. Pharmacol. 3 (1) (2024) 44–56.

[41] C.Y. Jia, J.Y. Li, G.F. Hao, G.F. Yang, A drug-likeness toolbox facilitates ADMET study in drug discovery, Drug Discov. Today 25 (1) (2020) 248–258, https://doi.org/10.1016/j.drudis.2019.10.014.

[42] L. Fu, S. Shi, J. Yi, N. Wang, Y. He, Z. Wu, J. Peng, Y. Deng, W. Wang, C. Wu, A. Lyu, X. Zeng, W. Zhao, T. Hou, D. Cao, ADMETlab 3.0: an updated comprehensive online ADMET prediction platform enhanced with broader coverage, improved performance, API functionality and decision support, Nucleic Acids Res. 5 (52) (2024) W422–W431, https://doi.org/10.1093/nar/gkae236. W1.

[43] G. Englert, NMR of carotenoids-new experimental techniques, Pure Appl. Chem. 57 (1985) 801–821.

[44] G. Englert, NMR spectroscopy, in: G. Britton, S. Liaaen-Jensen, H. Pfander (Eds.), Carotenoids, Vol 1B: Spectroscopy, Birkhaüser, 1995, pp. 147–260. Basel.

[45] S.-Q. Pi, H.-Y. Jiang, D.-W. Zhai, K.-L. Wang, Synthesis of β-apo-8'-carotenoic acid ethyl ester, J. Chem. Eng. Chin. Univ. 28 (6) (2014) 1340–1344, https://doi.org/10.3969/j.issn.1003-9015.2014.06.025.

[46] H. Hashimoto, Y. Miki, M. Kuki, T. Shimamura, H. Utsumi, Y. Koyama, Isolation by high-pressure liquid chromatography of the *cis-trans* isomers of β-apo-8′-carotenal. Determination of their S_0-State configuration by NMR spectroscopy and prediction of their S_1- and T_1- state configurations by transient raman spectroscopy, J. Am. Chem. Soc. 115 (1993) 9216–9225.

[47] V. Kuete, Potential of Cameroonian plants and derived-products against microbial infections: a review, Planta Med. 76 (2010) 1–13.

[48] M.A. Hossain, S. Sultana, M.M. Alanazi, H. Hadni, A.R. Bhat, I. Hasan, M. A. Kawsar, *In vitro* antimicrobial, anticancer evaluation, and *in silico* studies of mannopyranoside analogs against bacterial and fungal proteins: acylation leads to improved antimicrobial activity, Saudi Pharm. J. 32 (6) (2024) 102093, https://doi.org/10.1016/j.jsps.2024.102093.

[49] Z. Wang, Y. Zheng, Y. Hu, L. Yang, X. Liu, R. Zhao, M. Gao, Z. Li, Y. Feng, Y. Xu, N. Li, J. Yang, Q. Wang, L. An, Improvement of antibacterial activity of polysaccharides via chemical modification: a review, Int. J. Biol. Macromol. 269 (Pt 2) (2024) 132163, https://doi.org/10.1016/j.ijbiomac.2024.132163.

[50] C. Borreby, E.M.S. Lillebæk, B.H. Kallipolitis, Anti-infective activities of long-chain fatty acids against foodborne pathogens, FEMS Microbiol. Rev. 47 (4) (2023) fuad037, https://doi.org/10.1093/femsre/fuad037.

[51] A. Jayawardena, A. Hung, G. Qiao, E. Hajizadeh, Lipidation-induced bacterial cell membrane translocation of star-peptides [Pre-print], https://arxiv.org/abs/2505.06447, 2025.

[52] E. Bereczki, I. Györkei, P. Walther, K.J. Szabó, G. Tóth, Natural apocarotenoids and their synthetic glycopeptide conjugates inhibit SARS-CoV-2 replication, Pharmaceuticals 14 (11) (2020) 1111, https://doi.org/10.3390/ph14111111.

[53] F. Ahmmed, A.U. Islam, Y.E. Mukhrish, Y.E. Bakri, S. Ahmad, Y. Ozeki, S.M. A. Kawsar, Efficient antibacterial/antifungal activities: synthesis, molecular docking, molecular dynamics, pharmacokinetic, and binding free energy of galactopyranoside derivatives, Molecules 28 (1) (2023) 219, https://doi.org/10.3390/molecules28010219.

[54] D.F. Berhe, G.T. Beyene, B. Seyoum, M. Gebre, K. Haile, M. Tsegaye, M.T. Boltena, E. Tesema, T.C. Kibret, M. Biru, D.S. Siraj, D. Shirley, R. Howe, A. Abdissa, Prevalence of antimicrobial resistance and its clinical implications in Ethiopia: a systematic review, Antimicrob. Resist. Infect. Control 10 (2021) 168, https://doi.org/10.1186/s13756-021-00965-0.

[55] S. Woo, L. Marquez, W.J. Crandall, C.J. Risener, C.L. Quave, Recent advances in the discovery of plant-derived antimicrobial natural products to combat antimicrobial resistant pathogens: insights from 2018–2022, Nat. Prod. Rep. 40 (2023) 1271–1290, https://doi.org/10.1039/D2NP00090C.

[56] X. Liu, J. Shen, K. Zhu, Antibacterial activities of plant-derived xanthones, RSC Med. Chem. 13 (2022) 107–116, https://doi.org/10.1039/D1MD00351H, 2022.

[57] P. Angelini, Plant-derived antimicrobials and their crucial role in combating antimicrobial resistance, Antibiotics 13 (8) (2024) 746, https://doi.org/10.3390/antibiotics13080746.

[58] T. Karim, M.H. Almatarneh, S. Rahman, A.N. Alodhayb, H. Albrithen, MdM. Hossain, S.M.A. Kawsar, R.A. Poirier, K.M. Uddin, *In silico* prediction of antibacterial activity of quinolone derivatives, ChemistrySelect 9 (36) (2024) e202402780, https://doi.org/10.1002/slct.202402780.